

Article

Recharge of River Water to Karst Aquifer Determined by Hydrogeochemistry and Stable Isotopes

Yi Guo ^{1,2,3} , Dajun Qin ^{1,2,3,4,*}, Jie Sun ^{1,2,3}, Lu Li ^{1,2,3}, Fulin Li ⁵ and Jiwen Huang ⁵

¹ Key Laboratory of Shale Gas and Geoenvironment, Institute of Geology and Geophysics, Chinese Academy of Sciences, Beijing 100029, China; cugguoyi@163.com (Y.G.); jie.s@mail.iggcas.ac.cn (J.S.); liliuiggcas@sina.cn (L.L.)

² Institutions of Earth Science, Chinese Academy of Sciences, Beijing 100029, China

³ University of Chinese Academy of Sciences, Beijing 100049, China

⁴ Academician Zhaiming Guo working station, Sanya University, Hainan 572000, China

⁵ Shandong Provincial Water Resources Research Institute, Ji'nan 250013, China; fulinli@126.com (F.L.); sdskyhjw@126.com (J.H.)

* Correspondence: qindj@mail.iggcas.ac.cn; Tel.: +86-010-8299-8589

Received: 23 January 2019; Accepted: 28 February 2019; Published: 7 March 2019



Abstract: The Jinan Karst Spring System in Shandong province, China, has suffered to maintain groundwater level and spring flowing for decades. Recharge of river water to karst aquifer in Jinan is important for the outflowing of four large karst springs in the city center. Field investigations were conducted for two times in May and October, 2015, respectively and water samples were collected for hydrogeochemical and isotopic measurements. Results showed that (a) the water type was predominantly Ca-HCO₃-SO₄ for karst groundwater, and Ca-Mg-SO₄ for river water; (b) the concentration of HCO₃⁻ and NO₃⁻ in karst groundwater were higher than that in river water, in contrast, the concentration of SO₄²⁻ and K⁺ in karst groundwater were lower than that in river water; (c) the δ²H and δ¹⁸O values with average of −51.2‰ and −6.6‰ for river water is more enriched than the values in groundwater samples (−59.1‰ and −8.3‰), in that river experienced evaporation in the upstream reservoir; (d) Based on the distribution pattern of δ¹⁸O, groundwater near river bank was found to be recharged from river water and found a preferential flow path in karst aquifer situated from Dongkema to Manzizhuang near the river bank. This study provides useful information for understanding of the hydraulic connection between river water and karst aquifer, and benefit the protection and management of water resources.

Keywords: recharge; streambed; hydrogeochemistry; isotope; karst aquifer; Jinan

1. Introduction

The evaluation of effect of river water recharge on karst aquifers has double significances: the scientific one in terms of the relationship between river water and karst aquifers and the applied one in terms of the assessment and protection of karst water resources. However, it is not easy to identify the effect of river water infiltration through the streambed on karst groundwater due to the complex hydrogeological conditions of karst systems [1,2]. On one hand, the karst aquifer comprises a pattern of triple porosity, the matrix, fractures and conduits, which causes a high degree of heterogeneity on the hydraulic conductivity [3–7] and make it difficult to identify the flow paths and spatial effect areas of river water recharge in karst aquifers [8]. On the other hand, the recharge from the intermittent river is seasonally variable [9–11], which makes it difficult to reveal the temporal effect of river water recharge on karst groundwater [1,12].

Traditional hydrogeological investigations such as water level monitoring and river flow measurement result in uncertainty in evaluating the effect of river water recharge on karst groundwater

due to the heterogeneity of karst aquifers [1,2,13,14]. The distinguishing different characteristics of hydrogeochemical and/or isotope tracers between river water and karst groundwater provide a reliable method to evaluate the river water recharge on karst groundwater [15]. Hydrogeochemistry can not only identify the recharge from river water in karst aquifer [15], but can also reveal the possible hydrogeochemical processes underlying the recharge of river water based on the kinetic study of carbonate dissolution/precipitation [13,15,16]. In addition, inverse hydrogeochemical modeling can quantitatively study the theoretical mass transformation along the flow paths [17].

$\delta^2\text{H}$ and $\delta^{18}\text{O}$ are regarded as ideal natural tracers for quantitatively identifying the interaction between river water and groundwater [9,18,19]. On one hand, the $\delta^2\text{H}$ and $\delta^{18}\text{O}$ are only altered by physical processes such as diffusion, mixing, and evaporation under low temperature conditions [14]. On the other hand, river water usually has more enriched $\delta^2\text{H}$ and $\delta^{18}\text{O}$ values due to evaporation, compared with that in groundwater [13,15,20]. Except for the stable isotope, the concentration of ^{222}Rn in surface waters is generally less than 100 pCi/l, resulting from air degassing, while the concentration of ^{222}Rn is about 100 to 1000 pCi/l in groundwater [21]. The different ^{222}Rn concentration in surface water and groundwater also makes ^{222}Rn useful for tracing river water infiltration into groundwater [9,22]. Multi-tracers analyses (major ions, stable isotopes, and ^{222}Rn) are useful tools for delineating the flow paths of river water inflow [15].

Two of the most used multivariate statistical analyses are hierarchical cluster analysis (HCA) and principal component analysis (PCA) [2,23]. HCA enabled the classification of water samples into distinct groups based on their hydrochemical characteristics. On the other hand, PCA offers a better understanding about the factors for water quality [24,25].

The regional groundwater water level in Jinan karst system has decreased strongly, driven by exploitation, which has led to the karst springs in the city center drying occasionally in recent decades. In order to protect the karst springs, water from upstream reservoirs was drawn off artificially into the streambed of Yufu River from April to August in 2015. The river water infiltrated into the karst aquifer through the seepage section along the streambed, and formed a recharge for the Jinan karst system. This study is designed to investigate the effect of the recharge from the streambed of Yufu River on the karst groundwater in May (in the process of recharge) and October (after the recharge).

The purposes of this study include: (1) reveal the temporal and spatial effect of river water infiltration; (2) quantitate the fraction of river water in the karst aquifer; and (3) identify the flow path of infiltrated river water and reveal the hydrogeochemical processes along the flow path. We think this study will provide an improved understanding of the hydraulic connection between river and karst aquifer, and benefit the local water resource management.

2. Study Area

Jinan city is the capital of Shandong province, China, is located between the longitude of $116^{\circ}11'$ to $117^{\circ}44'$ E and the latitude of $36^{\circ}01'$ to $37^{\circ}32'$ N, with a total area of 8177 km² (Figure 1). In geomorphology, Jinan city is located in the north of the Mount Tai anticline, characterized by mountainous area in the southern part, inclined piedmont plain in the central part, and alluvial plain in the northern part (Figure 1). The climate is semi-arid continental monsoon climate, with cold, dry winters and hot, wet summers. Air temperature ranges from -1.4°C in January to 27.4°C in July, with mean temperature of 14.2°C . The annual mean precipitation is 642 mm, of which around 75% occurs from June to September. The annual mean evaporation is 1476 mm.

The Jinan karst system is located in the central part of Jinan. Archaean metamorphic rocks are the base and outcrop in the south of the catchment, and overlaid by Cambrian and Ordovician carbonate rocks to the north. The limestone and dolomites are massive and well jointed, with a stratigraphic thickness of 1300–1400 m. The Cambrian strata are composed of thick-bedded limestone, argillaceous limestone, and dolomite limestone, and the Ordovician strata are characterized by the inter-bed of limestone and shale. They dip away from the metamorphic rocks at angles varying from 5° to 10° in the dip direction of NW 20° . Intrusive magmatic rocks (diorite and gabbro) of the Yanshan epoch in

the Mesozoic are located in the top of the Ordovician strata in the north, and the intrusive rocks are buried mostly by Quaternary sediments (Figure 1).

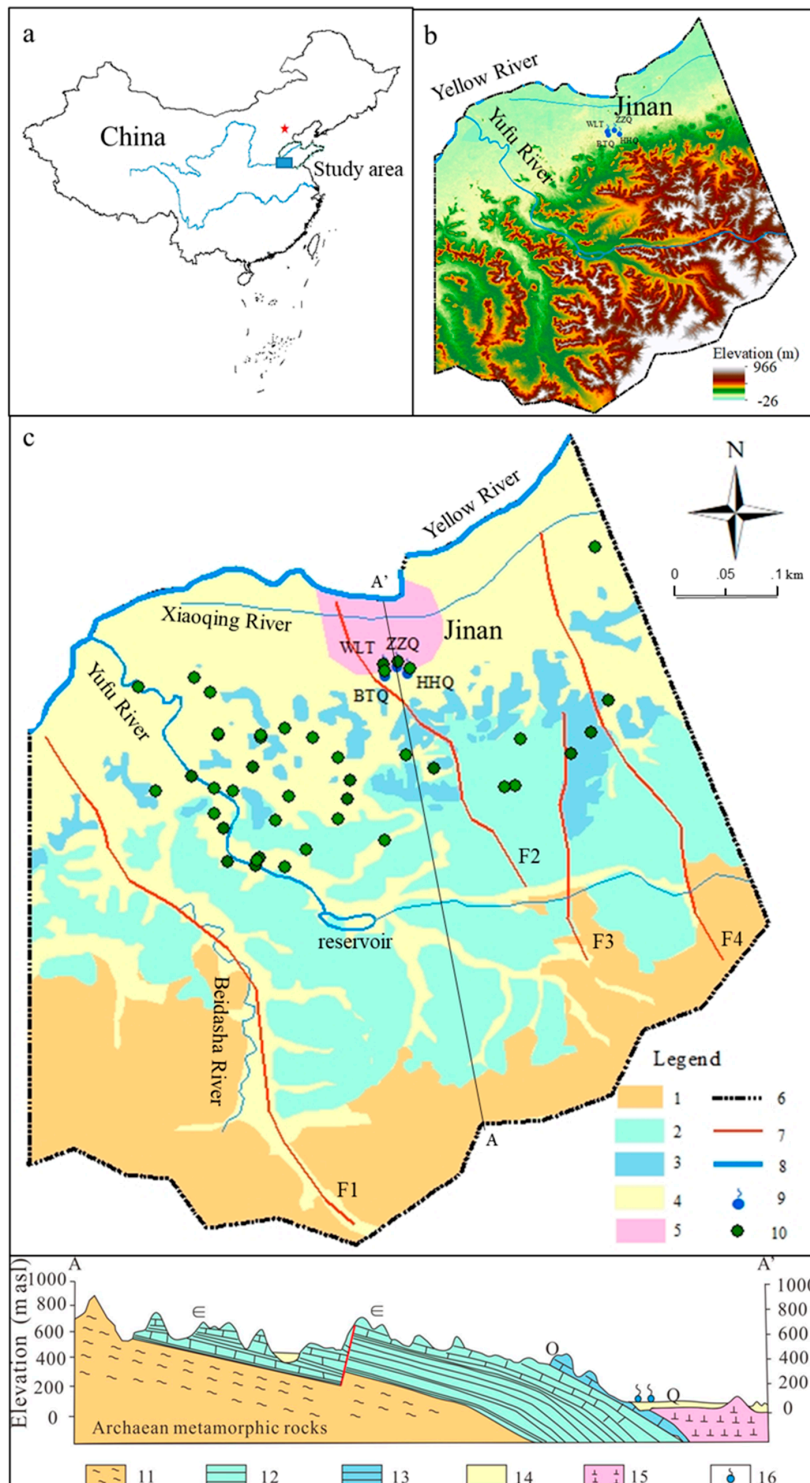


Figure 1. Location, sampling sites and hydrogeological map of Jinan karst system. (a) Location of the study area, (b) Topographic map of the study area. (c) Hydrogeological map of the Jinan karst system. (1, 11: Archaean metamorphic rocks; 2, 12: Cambrian limestone; 3, 13: Ordovician limestone; 4, 14: Quaternary sediments; 5, 15: magmatic rocks; 6: the range of study area; 7: fault; 8: river; 9, 16: spring; 10: sampling sites. A-A' in Figure c: geological cross section).

The karst aquifers consist of Cambrian and Ordovician carbonate rocks, with the hydraulic conductivity ranges from 0.05 m/day to 120 m/day [26]. Groundwater is tending to move from the south toward the north (similar to the dip direction of strata) and is hindered by the intrusive rocks to form discharge areas. In the city of Jinan, 108 springs occurred in an area of 2.6 km², of which Baotu Spring, Black-tiger Spring (Heihu Spring), Pearl Spring and Five-dragon Springs are the most well-known. The total discharge of springs was in the range from 3×10^5 to 4×10^5 m³/day in the 1960s, with the maximum value of 5×10^5 m³/day in 1962. Springs stopped flowing at the first time in 1973 and later on, zero flow occurred in 1982, 1989 and 2000–2002 due to the over-exploitation of groundwater. In order to restore the flow of these karst springs for environment and tourism, municipal water supply wells were switched off and river water has been drinking water as replacement. Flow of Baotu spring and Heihu spring has been restored since September 2003.

Precipitation is the main recharge source of the karst aquifer (Figure 2), with a supply module of more than 20 m³/a.km². Spring water level responds within 5 days when the total precipitation of 10 days is more than 18 mm [27]. Yufu River is another important recharge source of the karst aquifer [28,29], which originates in the southern mountains and flows in a northerly direction for about 65 km with a watershed of approximately 1510 km². The streambed of Yufu River is dry in recent decades, strongly driven by climate change (warmer and drier) and human activities (water withdrawal from rivers, groundwater exploitation, etc.). In the dry season, the water in Yufu River is possibly charged by water transported from upstream reservoirs, the Yellow River, and/or the Yangtze River through the South-to-North Water Diversion Project. The total volume of transported water was 4347×10^4 m³ in 2015 (data obtained from the website (<http://www.whssk.com>)). The maximum monthly volume of transported water was 2127×10^4 m³ in August, 2015. The transported water infiltrates into the karst aquifer under the leakage section of the streambed and forms a recharge. The volume of leakage water from Yufu River was 1.02×10^8 m³ in 1963. The maximum leakage section of Yufu River occurs at the CuiMa and PanCun sections, with 4.1–4.8 m³/s.

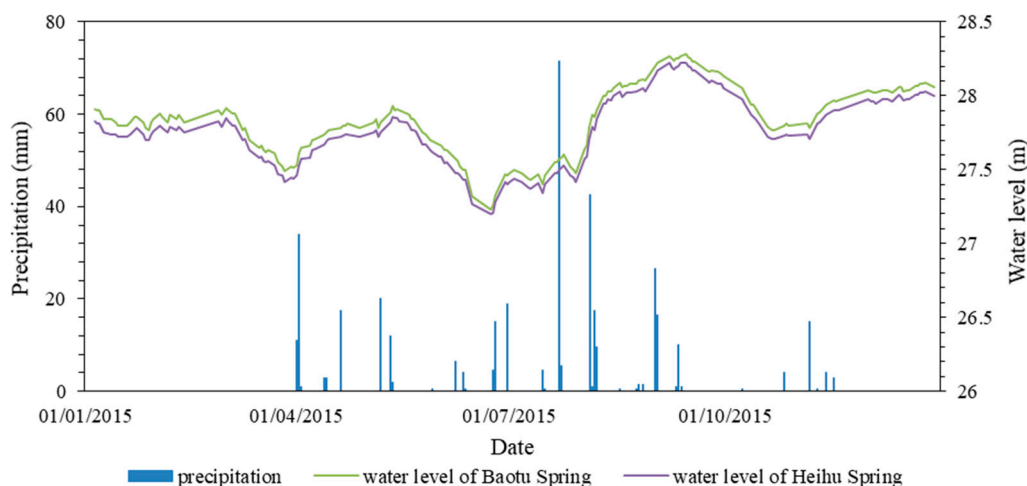


Figure 2. The plot of daily water levels of Baotu Spring and Heihu Spring, monthly precipitation, and monthly water flow of Yufu River in 2015.

3. Methods

In order to evaluate the effect of recharge from Yufu River on Jinan karst aquifer, two hydrogeochemical and isotopic investigations were conducted in May and October in the year of 2015, respectively. In total, 58 water samples were collected, with 28 samples (24 groundwater samples, 2 spring samples, and 2 river water samples) collected in May and 30 samples (26 groundwater samples and 4 spring samples) collected in October. River water samples were collected using the grab technique, and groundwater samples were collected from public supply wells after purging a minimum of three estimated casing volumes. The water samples were filtered through a 0.45 µm membrane

filter after sampling. Samples for cation analysis were stabilized by adding 1% HNO₃ immediately after filtration. The hydrogeochemical samples were collected in high density polyethylene bottles, which were pre-cleaned with 5% HNO₃ and deionized water. Samples for δ¹⁸O and δ²H measurement were sealed in 50 mL glass bottles using gas-tight caps. Samples for ²²²Rn were sealed in 100 mL glass bottles.

Water temperature, pH, and electrical conductivity (EC) were measured in the field during sampling using WTW portable multi-parameter instrument (Multi 340i/SET), with the precision of ±0.1 °C for temperature and ±1 µs/cm for EC. The major ion (SO₄²⁻, NO₃⁻, Cl⁻, Ca²⁺, Mg²⁺, Na⁺, and K⁺) were measured using ion chromatography (Dionex DX-120 Ion Chromatograph, Thermo Fisher Scientific, Washington, DC, USA) with analytical precision ±5%. HCO₃⁻ was analyzed by titration with 0.05 M HCl and methyl orange as an indicator. Water stable isotopes (²H/H and ¹⁸O/O) were measured using the Finnigan MAT 253 mass spectrometer (Scientific Instrument Services, Inc., Ringoes, NJ, USA). The results were reported in δ‰ referenced to VSMOW (Vienna Standard Mean Ocean Water). The measurement precision for δ²H and δ¹⁸O was ±1.0‰ and ±0.2‰, respectively. The ²²²Rn was measured using the RAD-7 environment radon measurement instrument (Division of Instrument Development of BRIUC, Beijing, China), with a measurement range of 0.003–100 Bq/L and a measurement precision of ±5%. All chemical and isotopic analyses were performed at the Institute of Geology and Geophysical, Chinese Academy of Sciences (IGG-CAS). The in situ parameters, together with analytical chemical parameters of the 58 water samples, are listed in Table 1, and the δ¹⁸O, δ²H, and ²²²Rn concentration of water sample are presented in Table 2.

Table 1. List of the field and analytical data as well as the results of some hydrochemical calculations (saturation indexes and water type).

Samplecode	Month	Temp °C	pH	HCO ₃ mg/L	SO ₄ mg/L	NO ₃ mg/L	Cl mg/L	Ca mg/L	Mg mg/L	Na mg/L	K mg/L	SIc	SI _d	SI _g	Water Type
JN1	May	18.1		311.3	111.2	81.7	32.5	97.1	9.2	11.7	1.5	-0.07	-0.91	-1.48	Ca-HCO ₃ -SO ₄
JN29	October	15.3	7.71	346.1	90.2	71.5	27.4	126.7	8.3	8.5	0.7	0.05	-0.88	-1.47	Ca-HCO ₃ -SO ₄
JN2	May	17.4		301.2	93.3	79.4	37.8	126.4	8.7	10.8	0.4	0.02	-0.89	-1.46	Ca-HCO ₃ -SO ₄
JN38	October	16.8	7.36	300.3	78.2	70.6	33	118.2	9.2	11	0.4	-0.01	-0.90	-1.55	Ca-HCO ₃ -SO ₄
JN3	May	19.1		255.7	110.6	53.6	26.8	56.3	14.4	17.6	3.2	-0.36	-1.04	-1.67	Ca-HCO ₃ -SO ₄
JN37	October	16.3	7.45	250.4	92	43.1	21.8	89.3	12.7	13.4	1.3	-0.20	-1.03	-1.56	Ca-HCO ₃ -SO ₄
JN4	May	19.4		208.3	162.7	19.6	67.4	87.6	14.3	51.8	3.6	-0.27	-1.06	-1.36	Ca-Na-HCO ₃ -SO ₄
JN35	October	14.9	7.7	190.4	136.7	9.2	48	77.8	14.2	28.1	2.1	-0.40	-1.34	-1.44	Ca-HCO ₃ -SO ₄
JN36	October	16.3	8.02	197.6	120.1	9.4	43	74.5	13.4	25.5	2	-0.38	-1.28	-1.51	Ca-HCO ₃ -SO ₄
JN5	May	19.2		326.8	107.3	82.7	79.5	103.4	17.9	21.2	0.4	-0.02	-0.53	-1.50	Ca-HCO ₃ -Cl-SO ₄
JN33	October	15.9	7.62	322.7	84.7	66.5	60.9	117.2	16.8	19.5	0.4	-0.01	-0.64	-1.54	Ca-HCO ₃
JN6	May	17.8		248.5	130.1	38.9	34.1	102.8	15.5	15.2	0.9	-0.14	-0.86	-1.39	Ca-HCO ₃ -SO ₄
JN31	October	17.6	7.66	242.6	99.9	32	24.7	83	13.8	13.1	1.1	-0.23	-0.99	-1.56	Ca-HCO ₃ -SO ₄
JN7	May	17.9		221.8	130.3	25.8	63.9	99.1	15.3	31.9	2.3	-0.21	-0.97	-1.4	Ca-HCO ₃ -SO ₄ -Cl
JN8	May	18.4		213.4	132.4	27.1	72.5	95.7	15.1	40	1.4	-0.23	-1.01	-1.41	Ca-Na-HCO ₃ -SO ₄
JN32	October	17.7	7.59	226.1	101.3	23.6	37.6	81.5	13.8	19.2	1.3	-0.26	-1.05	-1.55	Ca-HCO ₃ -SO ₄
JN9	May	18.4		267.5	91.7	41.8	37.5	106.7	13.8	16.3	1.3	-0.08	-0.79	-1.52	Ca-HCO ₃ -SO ₄
JN42	October	16.1	7.73	278.7	80.9	33.8	28.5	92.4	13.3	12.8	0.4	-0.14	-0.91	-1.61	Ca-HCO ₃ -SO ₄
JN10	May	14.7		251.1	146.8	48.6	29.1	69.1	12.2	18.3	2.7	-0.35	-1.26	-1.47	Ca-HCO ₃ -SO ₄
JN30	October	16.4	7.48	253.7	107.8	47.3	23.2	92.9	11.7	14.4	2	-0.19	-1.05	-1.49	Ca-HCO ₃ -SO ₄
JN11	May	19.1		188.8	140	81.4	49.7	138.5	19.7	19.7	1.3	-0.14	-0.85	-1.28	Ca-HCO ₃ -SO ₄
JN39	October	16.5	7.62	287.7	118.4	81.6	49.4	120.6	19	16.4	0.5	-0.05	-0.67	-1.40	Ca-HCO ₃ -SO ₄
JN12	May	17.4		310.7	149.9	66.1	52.7	151	15.1	27.3	1.2	0.08	-0.06	-1.23	Ca-HCO ₃ -SO ₄
JN13	May	17.1		345.1	136.1	103.2	58.2	156	14.9	24.4	1.3	0.13	-0.53	-1.27	Ca-HCO ₃ -SO ₄
JN14	May	17.6		303.8	138.3	79.7	140.4	157.2	21.7	28.2	1.4	0.08	-0.45	-1.27	Ca-HCO ₃ -Cl-SO ₄
JN40	October	15.8	7.42	299.2	102.2	66.9	40.3	118.3	13.6	18.7	0.3	-0.04	-0.80	-1.45	Ca-HCO ₃ -SO ₄
JN15	May	18.8		295.2	62.8	41.6	31	99.3	14.8	14.9	1.4	-0.05	-0.67	-1.70	Ca-HCO ₃
JN41	October	19.1	7.48	294.5	56.7	36.5	24.7	87.1	14.6	11.6	0.5	-0.10	-0.70	-1.78	Ca-HCO ₃
JN19	May	18.1		454.3	84.2	113.7	118.5	154.5	17.5	28	1.7	0.25	-0.19	-1.49	Ca-HCO ₃ -Cl
JN51	October	14	7.62	277	106.5	17.2	17.3	105.7	6.9	9.1	0.5	-0.12	-1.24	-1.42	Ca-HCO ₃ -SO ₄
JN20	May	21.6		274.1	136.8	35.4	24.6	97.8	19.5	4.5	0.5	-0.07	-0.54	-1.40	Ca-Mg-HCO ₃ -SO ₄
JN47	October	14	7.92	327.4	122.2	32	14.7	103.3	25.1	5.2	0.5	-0.08	-0.59	-1.42	Ca-Mg-HCO ₃ -SO ₄
JN16	May	17		342.3	90.2	55.5	37.7	44.4	27.9	80.7	3.5	-0.38	-0.73	-1.90	Na-Mg-Ca-HCO ₃ -SO ₄

Table 1. Cont.

Samplecode	Month	Temp °C	pH	HCO ₃	SO ₄	NO ₃	Cl	Ca	Mg	Na	K	SIc	SI _d	SI _g	Water Type
				mg/L	mg/L	mg/L	mg/L	mg/L	mg/L	mg/L	mg/L				
JN17	May	20.7		322.6	109.2	40.1	52.6	113.6	21	25.6	1.5	0.04	-0.36	-1.45	Ca-HCO ₃ -SO ₄
JN18	May	14.8		294.4	116.3	35	30.6	111.1	6.1	14.5	1.4	-0.08	-1.21	-1.39	Ca-HCO ₃ -SO ₄
JN21	May	16.6		252.0	29.0	1.0	24.4	72.7	31.3	70.0	1.8	-0.27	-0.67	-2.15	Ca-Na-Mg-HCO ₃
JN22	May	18.8		221.5	33.8	16.4	18.9	62.6	11.7	12.6	1.5	-0.33	-1.12	-2.08	Ca-HCO ₃
JN23	May	18.8		234.0	33.2	15.5	19.6	150.9	30.8	39.6	1.1	0.02	-0.38	-1.85	Ca-Na-Mg-HCO ₃
JN27	October	16.7	7.67	262.1	57.6	31.1	15	68.9	12.7	6.8	0.4	-0.27	-1.03	-1.84	Ca-HCO ₃ -SO ₄
JN28	October	16.5	7.44	234.4	128.5	72.1	48.1	114.4	24.8	16.1	0.4	-0.16	-0.75	-1.38	Ca-Mg-HCO ₃ -SO ₄
JN34	October	15.4	7.54	339.1	45.7	16.8	24.5	86.4	12.7	18	0.3	-0.09	-0.79	-1.86	Ca-HCO ₃
JN43	October	16.2	7.62	212.4	116.3	19	36.5	81.9	14.1	19.4	2	-0.31	-1.16	-1.49	Ca-HCO ₃ -SO ₄
JN44	October	15.1	7.8	259.4	79	49.7	7.7	97.5	6.7	7.8	0.9	-0.16	-1.28	-1.58	Ca-HCO ₃ -SO ₄
JN45	October	16.3	7.83	204.7	149.4	21.6	29	96.6	10.5	14.6	0.8	-0.27	-1.28	-1.33	Ca-HCO ₃ -SO ₄
JN46	October	17.7	7.59	231.6	94	20.8	39.1	79.7	14.7	18.7	1.3	-0.26	-1.01	-1.59	Ca-HCO ₃ -SO ₄
JN48	October	16.5	7.78	280.1	51.8	27	12.2	75.5	15.2	5.5	0.5	-0.20	-0.87	-1.85	Ca-Mg-HCO ₃
JN49	October	17.1	7.91	268	51.5	25.8	12.8	76	14.8	5.1	0.5	-0.21	-0.89	-1.85	Ca-Mg-HCO ₃
JN50	October	17.1	7.53	265.1	75.7	45.3	8.9	90.1	12.1	5.2	0.5	-0.16	-0.95	-1.64	Ca-HCO ₃ -SO ₄
JN52	October	17.9	7.6	270.5	76.8	30.9	14.8	81.8	17.1	7	0.5	-0.18	-0.78	-1.67	Ca-HCO ₃ -SO ₄
JN25	May	18.6		273.9	86	42.7	44.6	101.3	15.6	19.3	0.8	-0.09	-0.73	-1.57	Ca-HCO ₃ -SO ₄
JN53	October	17.5	7.48	271.1	72.7	34.5	35.7	78.4	13.3	16.3	0.9	-0.20	-0.93	-1.71	Ca-Na-HCO ₃ -SO ₄
JN26	May	18.5		297.2	107.7	50.4	57.5	114.1	17.3	27.9	1.8	-0.02	-0.60	-1.45	Ca-HCO ₃ -SO ₄
JN55	October	17.5	7.45	285	84.2	39.7	45.9	89.2	15	21.7	0.9	-0.14	-0.80	-1.62	Ca-HCO ₃ -SO ₄
JN24	May	19.2		279.3	68.4	35.5	47.2	77.1	21.2	17.6	2.6	-0.18	-0.64	-1.76	Ca-Mg-HCO ₃
JN54	October	18.1	7.56	333.2	72.7	22	38.8	60.8	13.2	23.8	1.1	-0.21	-0.83	-1.81	Ca-HCO ₃ -SO ₄
JN56	October	18	7.64	242.3	65.8	25.5	32	66.9	13.7	19.9	1.2	-0.30	-1.03	-1.80	Ca-HCO ₃ -SO ₄
JN57	May	22.2		144.4	133.7	10.7	33.3	51.7	15.1	19.6	3.2	-0.58	-1.39	-1.60	Ca-Mg-SO ₄ -HCO ₃
JN58	May	24.2		81.3	134.8	6.6	43.5	150.5	20.9	31	2.3	-0.37	-1.26	-1.25	Ca-Mg-SO ₄

The water type was calculated using AquaChem software (3.7) (waterloo hydrogeological, Kitchener, ON, Canada), the saturation index for calcite (SI_c), dolomite (SI_d), and gypsum (SI_g) were calculated by Phreeqc (version 3.3.12) (USGS, Reston, VA, USA), and Q-mode hierarchical cluster analyses (HCA) were performed on the major ions (HCO₃⁻, SO₄²⁻, NO₃⁻, Cl⁻, Ca²⁺, Mg²⁺, Na⁺ and K⁺) and δ¹⁸O and δ²H to group the samples using SPSS software (version 21) (IBM, New York, NY, USA). Before the HCA, the above parameters were standardized by calculating their z-scores, to ensure that each variable is weighted equally. Euclidean distance together with Ward's method for linkage were used to produce the distinctive groups. Results can be displayed as a tree diagram (dendrogram), which provides a visual summary of the clustering process by presenting a picture of the groups and their proximity.

Inverse hydrogeochemical modeling was done using the Phreeqc (version 3.3.12) to quantify the mass transfer along the water flow path. The mass transfer models are constrained by the concentrations of the dissolved constituents in initial and final waters, such as C, S, Ca, Mg, and CO₂. Calcite, dolomite, and gypsum were chosen as the major mineral phases. The uncertainty (global uncertainty) for water composition was 5%; in cases where the model could not produce a result, global uncertainty was increased by integer increments up to 20%.

Table 2. Isotope data of the water samples in Jinan.

Site	Code	Month	Rn	$\delta^{18}\text{O}$	$\delta^2\text{H}$	d-Excess
			Bq/L	‰	‰	‰
Groundwater						
	JN1	May	7.55	−8.93	−62.18	9.26
	JN29	October	10.78	−8.73	−61.42	8.42
	JN2	May	29.87	−8.97	−62.63	9.13
	JN38	October	26.85	−8.69	−61.64	7.88
	JN3	May	6.54	−8.13	−58.24	6.8
	JN37	October	20.53	−7.48	−55.77	4.07
	JN4	May	12	−6.89	−51.84	3.28
	JN35	October	31.53	−6.29	−50.04	0.28
	JN36	October	13.69	−6.01	−48.52	−0.44
	JN5	May	12.97	−8.79	−61.6	8.72
	JN33	October	14.9	−8.48	−61.43	6.41
	JN6	May	27.44	−7.91	−57.09	6.19
	JN31	October	19.38	−7.59	−55.91	4.81
	JN7	May	7.33	−7.68	−56.09	5.35
	JN8	May	6.71	−7.57	−55.19	5.37
	JN32	October	11.65	−7.35	−53.82	4.98
	JN9	May	7.24	−8.49	−60.35	7.57
	JN42	October	12.01	−8.41	−60.06	7.22
	JN10	May	6.63	−7.38	−53.01	6.03
	JN30	October	9.29	−7.21	−53.19	4.49
	JN11	May	10.29	−9.04	−62.34	9.98
	JN39	October	12.9	−8.68	−61.29	8.15
	JN12	May	34.3	−8.82	−61.3	9.26
	JN13	May	16.85	−8.79	−61.13	9.19
	JN14	May	24.42	−8.46	−60.42	7.26
	JN40	October	0	−8.77	−61.73	8.43
	JN15	May	21.31	−8.48	−60.57	7.27
	JN41	October	13.95	−8.55	−61.17	7.23
	JN19	October	20.87	−8.35	−57.51	9.29
	JN51	May	22.77	−7.57	−55.07	5.49
	JN20	May	1.34	−7.23	−46.6	11.24
	JN47	May	3.31	−8.17	−56.74	8.62
	JN16	May	33.86	−8.39	−59.33	7.79
	JN17	October	26.98	−8.18	−57.98	7.46
	JN18	May	40.26	−7.62	−53.76	7.2
	JN21	May	0.01	−8.73	−62.56	7.28
	JN22	May	29.83	−8.63	−61.84	7.2
	JN23	May	17.9	−8.79	−62.75	7.57
	JN27	October	11.97	−8.89	−61.9	9.22
	JN28	October	18.79	−8.58	−59.96	8.68
	JN34	October	40.11	−8.73	−63.4	6.44
	JN43	October	19.46	−6.83	−51.75	2.89
	JN44	October	12.17	−8.72	−60.3	9.46
	JN45	October	28.1	−7.23	−53.64	4.2
	JN46	October	17.1	−7.31	−54.48	4
	JN48	October	11.91	−9.01	−62.77	9.31
	JN49	October	11.33	−8.99	−62.99	8.93
	JN50	October	23.72	−8.82	−60.62	9.94
	JN52	October	38.33	−8.82	−61.56	9
	JN25	May	10.45	−8.3	−59.45	6.95
	JN53	October	6.85	−8.48	−60.68	7.16
	JN26	May	5.25	−8.33	−59.23	7.41
	JN55	October	4.3	−8.35	−59.7	7.1
	JN24	May	2.51	−8.89	−62.5	8.62
	JN54	October	5.25	−8.11	−59.25	5.63
	JN56	October	2.65	−8.2	−59.62	5.98
River water						
	JN57	May	1.46	−6.11	−46.79	2.09
	JN58	May	0.98	−5.9	−45.94	1.26

4. Results

4.1. Hydrogeochemistry

The temperature of groundwater samples ranged from 14.7 °C to 21.6 °C (18.2 °C on average, 1.46, standard deviation) in May and from 14.0 °C to 19.1 °C (16.5 °C on average, 1.17, standard deviation) in October, while the temperature of river water was on average 23.2 °C in May (1.00, standard deviation). HCO_3^- , SO_4^{2-} and Ca^{2+} constituted over 75% of the dissolved solids in groundwater. The HCO_3^- in the groundwater ranged from 189 mg/L to 454 mg/L in May and from 177 mg/L to 346 mg/L in October, which was obviously higher than that in river water (112.8 mg/L on average, 31.6 standard deviation). The SO_4^{2-} in groundwater showed wide range, from 29 mg/L to 163 mg/L in May and from 46 mg/L to 185 mg/L in October, the SO_4^{2-} in river water was averagely 134.3 mg/L (0.5, standard deviation). The Ca^{2+} in groundwater also showed wide range from 44 mg/L to 157 mg/L in May, and from 22 mg/L to 127 mg/L in October; the Ca^{2+} in river water was 51.1 mg/L (0.6 standard deviation). The NO_3^- in groundwater was on average 53.6 mg/L (28.7 standard deviation) with a maximum of 120 mg/L in May, and on average 41.3 mg/L (19.8 standard deviation), with the maximum value of 114 mg/L in October, obviously higher than that in river water (10.7 mg/L on averagely, 2.0 standard deviation).

The saturation index of calcite (SIc) ranged from -0.38 to 0.13 for groundwater in May and from -0.40 to 0.05 for groundwater in October (Figure 3a). According to the criterion of ± 0.1 , most groundwater samples were unsaturated with calcite. The saturation index of dolomite (SID) ranged from -1.26 to -0.06 for groundwater in May and from -1.34 to -0.59 for groundwater in October (Figure 3b). According to the criterion of ± 0.5 [30], groundwater samples were generally unsaturated with dolomite. The saturation index of gypsum ranged from -2.15 to -1.23 for groundwater samples in May and from -1.86 to -1.33 for groundwater samples in October, indicating that the groundwater samples were unsaturated with gypsum (Figure 3c). The SIc and SID for river water were less than that of groundwater (-0.48 and -1.33 , respectively), while the SIg for river water was similar to that of groundwater with a value of -1.43 .

The groundwater samples were generally located between the 1:2 and 1:4 line of $(\text{Ca}-\text{SO}_4)/\text{HCO}_3$ (Figure 3d), reflecting the dissolution of calcite and dolomite. The same result was also obtained from the ratio of Mg/Ca which ranged from 0.11 to 0.73, as the Mg/Ca ratio was 0.03 and 1 for calcite and dolomite, respectively (Figure 3e). The ratio of Na/Ca in both calcite and dolomite is low, 0.005 and 0.01, respectively. Thus, the high ratio of Na/Ca in groundwater samples indicated mixing with river water, as the water from Yufu River had a higher Na/Ca, around 0.7 (Figure 3f).

Based on hydrogeochemical data, the water type of most groundwater samples was Ca- HCO_3 - SO_4 , and a minority were Ca-Mg- HCO_3 - SO_4 , Ca-Na- HCO_3 - SO_4 , Ca- HCO_3 -Cl- SO_4 , Ca- HCO_3 - SO_4 -Cl, Ca-Na-Mg- HCO_3 , Ca-Mg- HCO_3 and Ca-Na- HCO_3 . The water type of river water was Ca-Mg- SO_4 (Figure 4).

4.2. Stable Isotopes

Among the collected water samples, river water had the most enriched $\delta^{18}\text{O}$ and $\delta^2\text{H}$ values, ranging from -6.11‰ to -5.9‰ and from -46.8‰ to -45.9‰ , respectively. On the other hand, river water had the lowest d-excess (between 1.26‰ and 2.09‰). River water samples plotted below the Global Meteoric Water Line (GMWL) ($\delta^2\text{H} = 8\delta^{18}\text{O} + 10$ [31]), indicating that the river water had undergone evaporative enrichment.

For groundwater in May, the $\delta^{18}\text{O}$ values ranged from -9.04‰ to -6.89‰ with an average of 8.3‰ and a standard deviation of 0.58. The $\delta^2\text{H}$ values ranged from -62.8‰ to -46.6‰ , with an average of -58.75‰ and a standard deviation of 3.93. The $\delta^2\text{H}$ - $\delta^{18}\text{O}$ relationship was $\delta^2\text{H} = 6.39\delta^{18}\text{O} - 5.74$ ($R^2 = 0.88$). The d-excess showed a range of 3.28‰ to 11.24‰ .

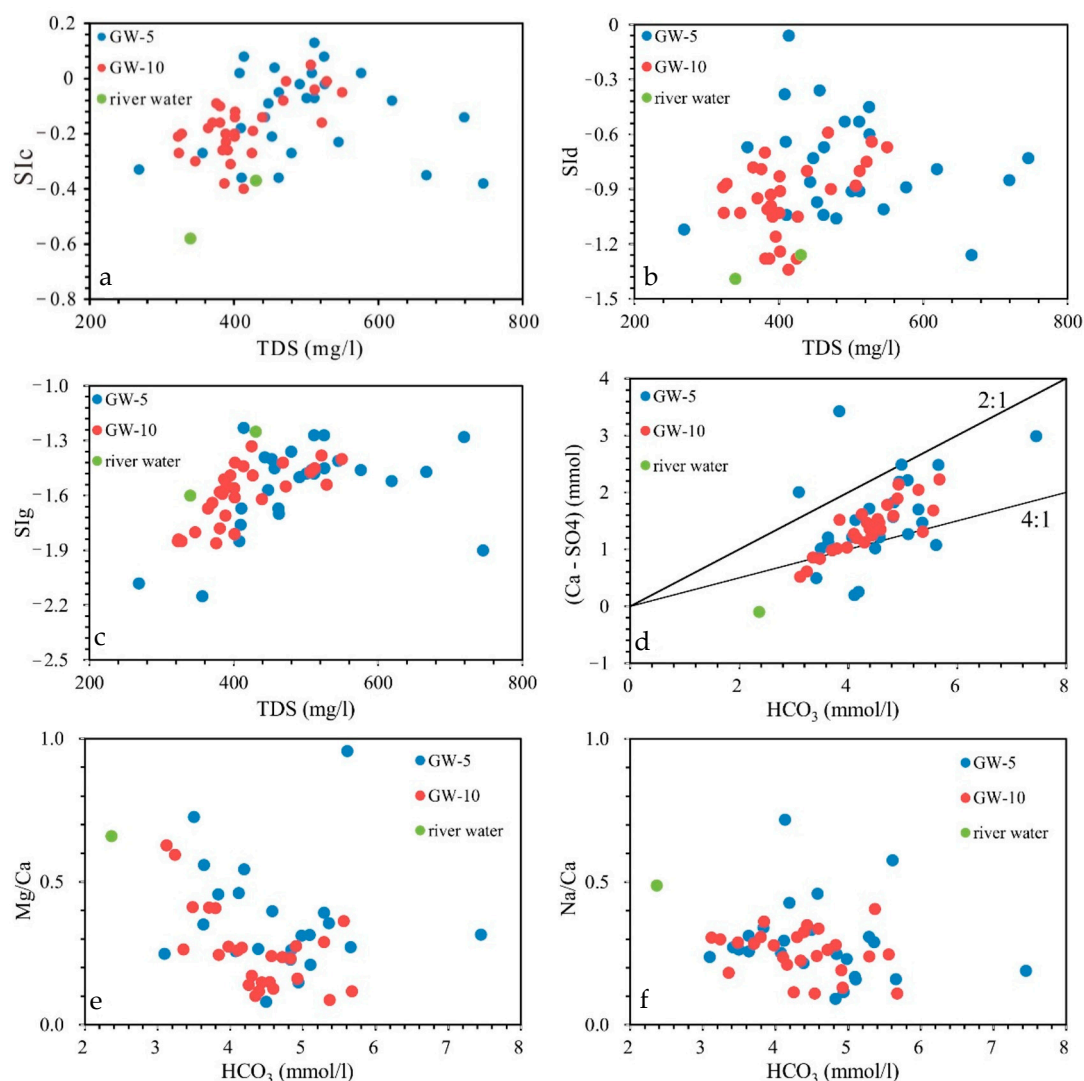


Figure 3. Relationship between TDS(Total dissolved solids) and saturation index of calcite (SIc) (a), TDS and saturation index of dolomite (SIld) (b), TDS and saturation index of gypsum (SIg) (c), HCO_3 and $(\text{Ca} - \text{SO}_4)$ (d), HCO_3 and Mg/Ca (e), and HCO_3 and Na/Ca (f) in groundwater and river water. (In this figure the following figures, the GW-5 represents the groundwater collected in May and GW-10 represents the groundwater collected in October 2015.)

For groundwater in October, the $\delta^{18}\text{O}$ values ranged from -9.01‰ to -6.00‰ , with an average of 8.1‰ and a standard deviation of 0.80. The $\delta^2\text{H}$ values ranged from -63.4‰ to -48.5‰ with an average of -58.4‰ and a standard deviation of 4.05. The $\delta^2\text{H} - \delta^{18}\text{O}$ relationship was $\delta^2\text{H} = 4.93\delta^{18}\text{O} - 18.40$ ($R^2 = 0.96$). The d-excess showed a range of -0.44‰ to 9.94‰ .

Two groups of groundwater were identified based on stable isotope values (Figure 5). Samples in group 1(G1) had low stable isotopic composition and were located around the GMWL. The stable isotope signatures of these samples showed little or no evaporative enrichment, which indicated these samples were mainly recharged by local precipitation. Samples in group 2 (G2) had elevated stable isotopic values, and were located below the GMWL with deviation direction toward to the river water samples. These signatures suggested that these samples were mixed with infiltrated river water, because the precipitation recharge did not show evaporative enrichment prior to recharging the aquifer. The sample collected in Longdong (JN20) was the only sample located above the global meteoric water line GMWL, reflecting the heterogeneous water flow in karst aquifer.

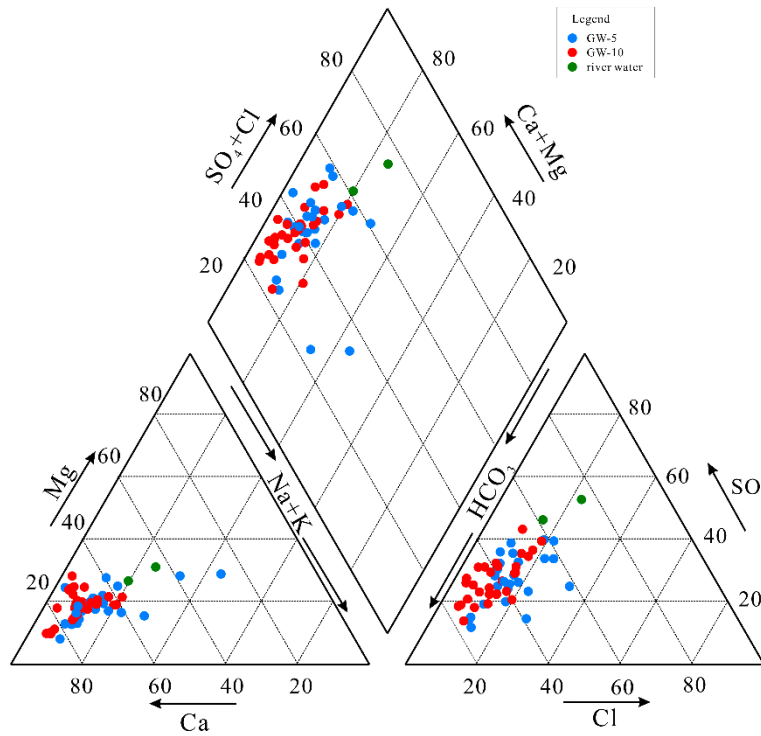


Figure 4. Piper diagram of water samples in Jinan.

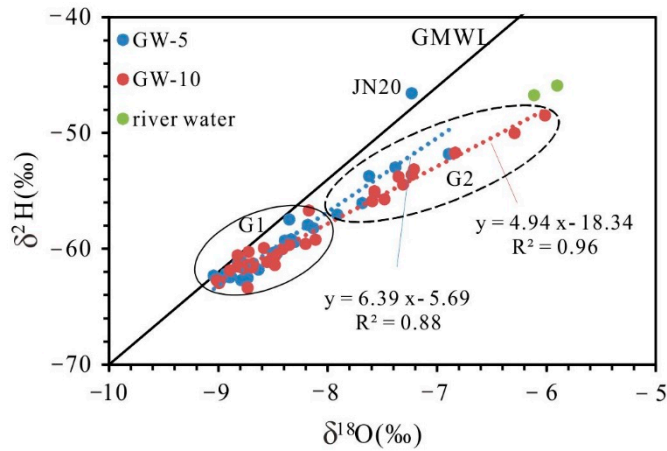


Figure 5. Plot $\delta^{18}\text{O}$ versus $\delta^2\text{H}$ for river water and karst groundwater in the study area (GMWL = global meteoric water line; LMWL = local meteoric water line).

4.3. ^{222}Rn

The average ^{222}Rn concentration in river water was 1.22 Bq/L, while the ^{222}Rn concentration in groundwater showed considerable variability, from 0.01 to 40.26 Bq/L in May and from 0 to 40.11 Bq/L in October. The groundwater samples were divided into three groups based on the relationship between ^{222}Rn and TDS, indicating different flow paths with different dynamic conditions. The groundwater samples in group 1 had a lower ^{222}Rn concentration, which was positively correlated with TDS. The groundwater samples in group 2 had higher ^{222}Rn concentration, which was also positively correlated with TDS. The two groundwater samples in group 3 had the highest ^{222}Rn (Figure 6).

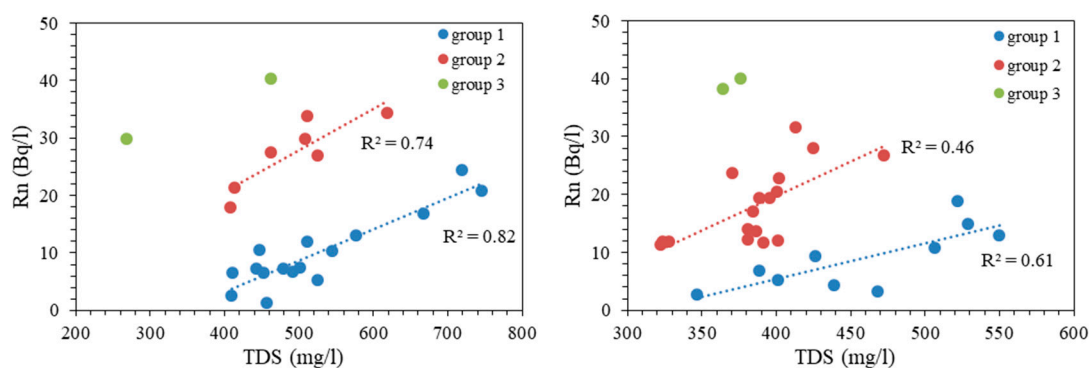


Figure 6. Relationship between ²²²Rn with TDS for groundwater in May (left) and October (right).

4.4. Hierarchical Cluster Analysis

Three groups (C1, C2, and C3) were obtained by hierarchical cluster analysis (HCA) for groundwater samples in May using a Euclidean distance of 15 (Figure 7). Table 3 presents the average values of chemical and isotope data in each group. The group C1 mainly consisted of the groundwater samples from the water source area (JN21/JN22/JN23) and karst springs (JN24/JN25/JN26), with lowest average TDS values of 431 mg/L. The groundwater samples from group C2 had the lowest HCO₃⁻, highest SO₄²⁻, and most enriched stable isotope. The groundwater samples in group C3 had the highest TDS of 610 mg/L with highest concentration of HCO₃⁻, SO₄²⁻, Ca²⁺, and ²²²Rn, and depleted stable isotope compositions.

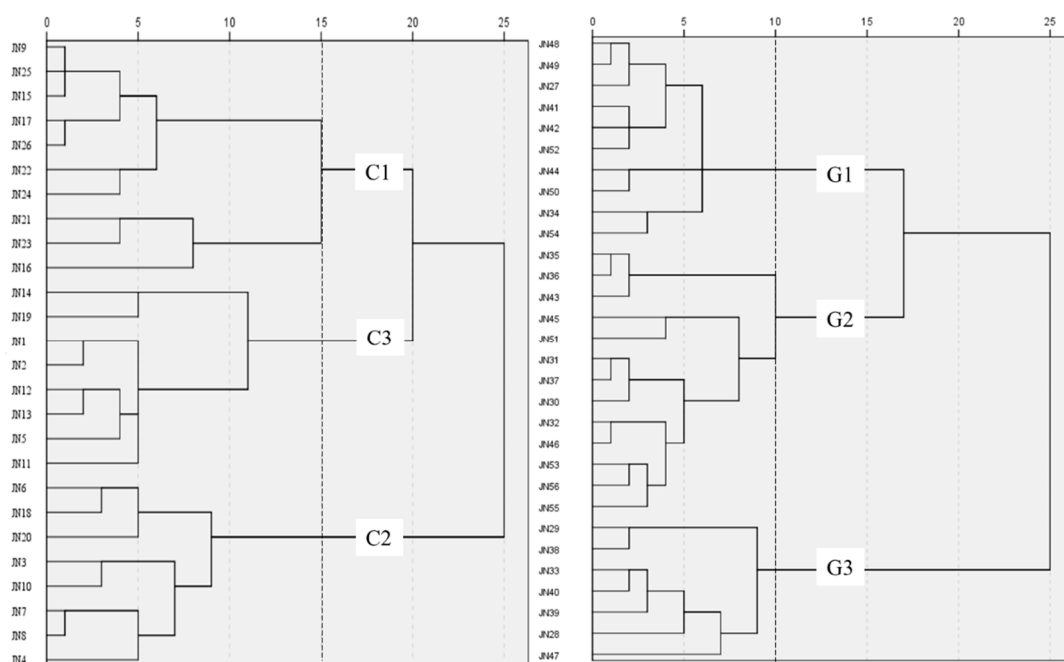


Figure 7. The HCA dendrogram of groundwater samples in May (left) and in October (right).

Table 3. The statistical results of clusters for groundwater samples from May.

	HCO ₃	SO ₄	NO ₃	Cl	Ca	Mg	Na	K	TDS	SIc	SI d	SIg	Rn	O	H
	mg/L											Bq/L	‰		
C1	279	71	34	37	94	21	32	2	431	-0.1	-0.60	-1.60	15.53	-8.52	-60.66
C2	246	133	36	44	90	14	24	2	466	-0.16	-0.82	-1.53	13.53	-7.55	-53.98
C3	318	120	86	71	136	16	21	1	610	-0.15	-0.92	-1.50	19.64	-8.77	-61.14

Similarly, three groups (G1, G2, and G3) were obtained for groundwater samples in October using a Euclidean distance of 10. Table 4 presents the average values of chemical and isotope data in each group. The groundwater samples in group G1 had the lowest average TDS value of 365 mg/L. The groundwater samples in group G2 had the lowest HCO_3^- , NO_3^- , highest SO_4^{2-} , Na^+ , least S1c, S1d and S1g, and most enriched stable isotope. The groundwater samples in group G3 had the highest average TDS of 508 mg/L.

Table 4. The statistical results of clusters for groundwater samples from October.

	HCO ₃	SO ₄	NO ₃	Cl	Ca	Mg	Na	K	TDS	S1c	S1d	S1g	Rn	O	H
	mg/L									Bq/L			‰		
G1	285	65	32	19	82	13	10	1	365	-0.2	-0.9	-1.7	18.1	-8.7	-61.4
G2	237	104	26	33	84	13	18	1	399	-2.6	-1.1	-13.9	15.9	-7.4	-54.8
G3	303	103	66	39	117	17	14	0	508	0.0	-0.7	-1.5	12.5	-8.6	-60.6

5. Discussion

5.1. The Temporal Effect of the Recharge

32 groundwater samples from 16 sites were collected in both May and October. Based on the hydrogeochemical, stable isotope, and ²²²Rn characteristics of these samples, there were four kinds of temporal evaluation mechanisms for karst groundwater (Figure 8).

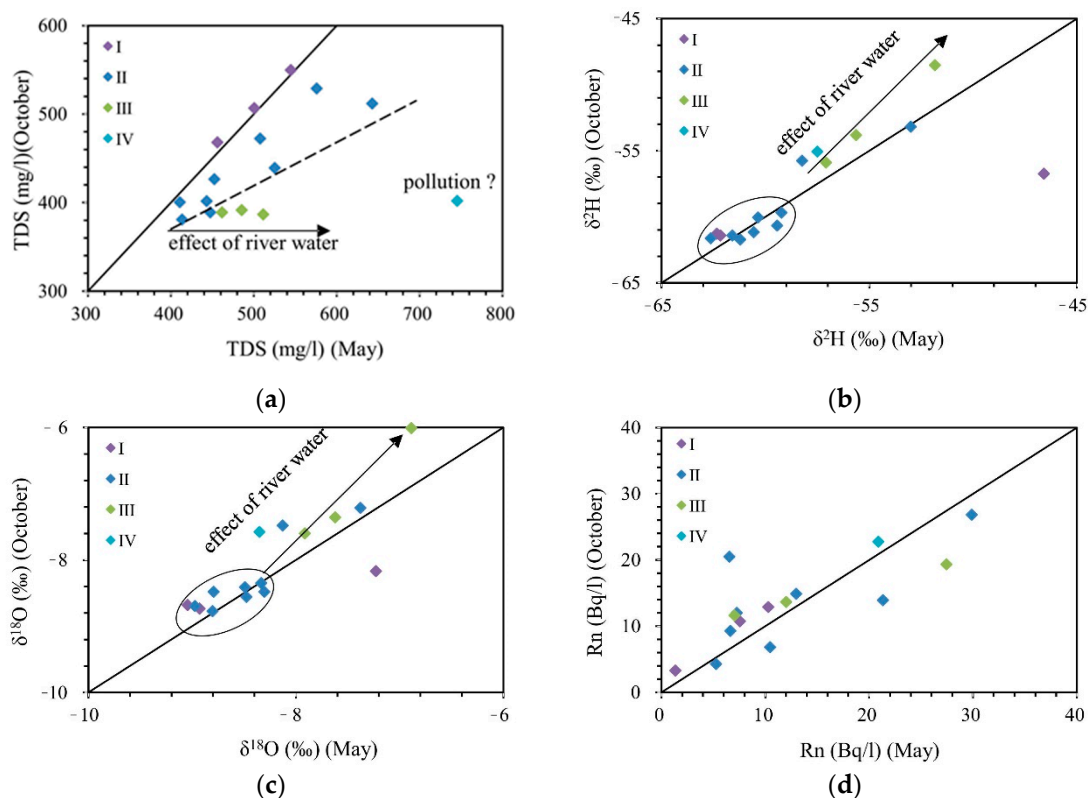


Figure 8. The relationships between TDS (a), $\delta^2\text{H}$ (b), $\delta^{18}\text{O}$ (c), and ^{222}Rn (d) for groundwater between May and October.

Type I: 3 sites located far away the streambed of Yufu River had similar TDS in May and October, did not show seasonal variation. Sample 20 was collected in Longdong, and had obviously enriched $\delta^{18}\text{O}$ and $\delta^2\text{H}$ in May, which may be due to the dependent water flow in May caused by the heterogeneity of the karst aquifer.

Type II: 9 sites from the regional scope had higher TDS in May than in October, and similar $\delta^{18}\text{O}$ and $\delta^2\text{H}$ composition without showing seasonal variation.

Type III: 3 sites located very close to the streambed of Yufu River also had higher TDS in May than in October, and the seasonal differences were more obvious than that in type II. In addition, these sites had higher $\delta^{18}\text{O}$ and $\delta^2\text{H}$ values than other sites, and the stable isotope values were more enriched in October than in May. The TDS and stable isotope signatures proved the temporal variations were mainly caused by the recharge from the streambed of Yufu River. The effect of river water recharge was more obvious in October than in May for karst groundwater in this study; this was consistent with the flow conditions of the fracture karst aquifers in North China.

Type IV: 1 site from the east of the study area had the highest TDS in May, which may be from mixing with other water bodies, such as pollution water.

The ^{222}Rn did not show regular variation, which may due to the complex seasonal dynamic changes of the water flow environment. The hydrogeochemistry and stable isotope signatures reveal that the river water recharge changes the temporal variation of karst groundwater. The temporal variation revealed there was lag time between river water recharge event and the responses from karst groundwater.

5.2. The Spatial Effect of the Recharge

The spatial effect of the recharge from the streambed could be revealed by the distribution of the groundwater samples. Figure 9 shows the distribution of groundwater samples based on the results from the hierarchical cluster analysis (HCA). According to Figure 9, the Jinan karst system can be divided into four zones.

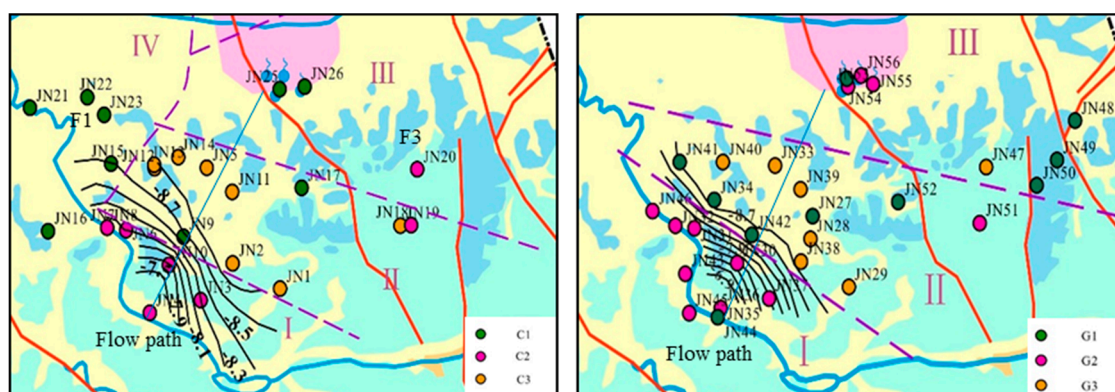


Figure 9. Distribution of groundwater samples based on the cluster analysis in May (left) and October (right) (black line is the isoline based on the $\delta^{18}\text{O}$ values of groundwater samples; the C1, C2, and C2 in May and G1, G2, and G3 in October are the clusters from the hierarchical cluster analysis).

Zone I is located close to the streambed of Yufu River. Samples in this zone are recharged by river water with lower HCO_3 , Si^{ic} and Si^{d} , higher SO_4 , and enriched $\delta^{18}\text{O}$ values compared with the groundwater in other zones.

Zone II is located in the middle area between the Yufu River and the karst springs in city center. Groundwater in this zone has both the highest TDS (groundwater samples in C3/G3) and the lowest TDS (groundwater samples in C1/G1). The different TDS concentration reflects the different recharge area, the higher one represents the water from the indirect recharge zone with a longer flow path, and the lower one represents the water from the direct recharge with a short flow path.

Zone III is located in the discharge area. Karst springs in this zone respond to the river water recharge immediately in the aspect of water level dynamic [27]. The average flow rate of karst groundwater is 100 m/day in Jinan by the tracer test. The distance between the springs in city center and the permeable section of the Yufu River is around 20 km; the shortest response time is 200 day, without consideration of the tortuosity factor. Therefore, the immediate responses of spring water

level to river water infiltration are the results of pressure waves, showing the hydraulic connection between the streambed and karst springs. The responses of hydrogeochemistry and isotope are the responses to the actual recharge with time tag [32]. Therefore, in respect to hydrogeochemistry and isotope, these springs belong to C1 in May, indicating they do not receive the river water recharge, of mixing with river water, and belong to G2 in October, reflecting the recharge from river water.

Zone IV is located in the northwest of Jinan city with several water resource sites. Groundwater in this zone has better quality with less TDS.

5.3. Hydrogeochemical Processes Along the Flow Paths

Based on the signatures of groundwater samples in different spatial zones, the main effect area of the river water recharge is around the streambed. The potential flow path of the river water recharge was identified by the counter line of $\delta^{18}\text{O}$ in groundwater, which was from Dongkema to Manzi to Shaoer, through Shanyao toward springs in city center (JN4 → JN10 → JN9 → JN5 → JN28/JN29 in May, and from JN35 → JN30 → JN42 → JN33 → JN53/JN54 in October). The hydrogeochemical processes along the flow path of river water recharge were complex and different in different zones (Figure 10).

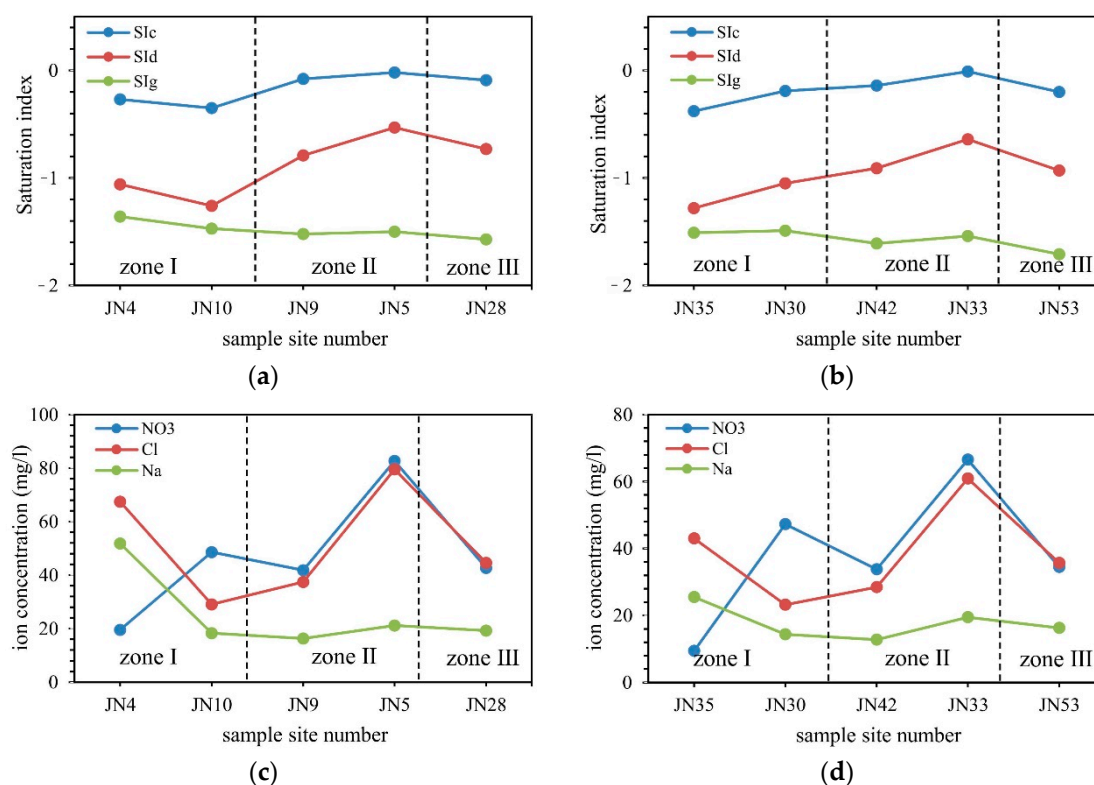


Figure 10. The variation of S1c, S1d, S1g, NO₃, Cl, and Na along the flow path of river water recharge (zone I, zone II, and zone III were obtained from the cluster analysis from Figure 9). (a) the variation of S1c, S1d, S1g along the flow path in May, (b) the variation of S1c, S1d, S1g along the flow path in October, (c) the variation of NO₃, Cl, and Na along the flow path in May, (d) the variation of NO₃, Cl, and Na along the flow path in October.

At the beginning of the flow path (zone I), from Dongkema to Manzi, the S1c, S1d, and S1g decreased in May (JN4 to JN10), while it increased in October (JN35 to JN30). In addition, Cl⁻ and Na⁺ decreased and NO₃⁻ increased in both May and October. The variations were mainly the results of mixing with the less mineral river water.

At the middle of the flow path (zone II), from Manzi to Shanyao, the S1c and S1d increased in May and October. The Na⁺ concentration did not show obvious variation, while the Cl⁻ and NO₃⁻

increased obviously. The variations of hydrogeochemistry were controlled by both river water mixing and natural water–rock interaction.

At the end of the flow path (zone III), from Shanyao to Baotu Spring, the SI_c , SI_d , and SI_g decreased in both May and October (JN5 to JN28 in May and JN33 to JN53); NO_3^- , Cl^- , and Na^+ also decreased, reflecting the fact that the water in discharge area is a mixture of water from different recharge area.

The quantitative variations of mineral phases along the flow paths were calculated by inverse hydrogeochemical modeling. For the streambed of Yufu River to springs in city center, the hydrogeochemical processes were complex and different in May and October (Table 5). In May, calcite dissolved first and then precipitated along the flow path, gypsum precipitated first and then dissolved along the flow path, and dolomite generally precipitated along the flow path. In October, calcite and dolomite dissolved first and then precipitated along the flow path, and gypsum was generally in the condition of precipitation along the flow path.

Table 5. The simulation results for the inverse hydrogeochemical model.

No.	Flow Path	Transferring Molar Concentration of Mineral Phase (mmol/L)				
		Calcite	Dolomite	Gypsum	Halite	CO ₂
May	JN4 → JN10	0.24	−0.09	−0.53	−1.33	1.08
	JN10 → JN9	0.57	−0.03	−0.12	0.03	−0.20
	JN9 → JN5	0.10	0.19	−0.06	0.53	0.93
	JN5 → JN28	−0.20	−0.11	0.00	−0.28	−0.83
	JN5 → JN29	−0.15	−0.04	0.23	0.11	0.23
October	JN35 → JN30	0.59	0.07	−0.07	−0.48	0.99
	JN30 → JN42	0.07	0.07	−0.28	−0.01	0.14
	JN42 → JN33	0.06	0.14	0.04	0.46	0.64
	JN33 → JN55	−0.24	−0.09	−0.28	−0.31	−0.55
	JN33 → JN56	−0.15	−0.07	−0.05	−0.07	−0.34

Notes: Positive means dissolution and negative indicates precipitation.

5.4. Quantify the Proportion of River Water in Groundwater

A two component mixing model was used to estimate the proportion of river water (ω) in groundwater, defined as:

$$\omega = \frac{c_g - c'_g}{c_g - c_r} \times 100\% \quad (1)$$

where c_g , c'_g , and c_r are the $\delta^{18}O$ values in the groundwater, groundwater without mixing with river water, and river water, respectively.

The $\delta^{18}O$ value of river water endmember was -6.0‰ , which was the average value of the $\delta^{18}O$ values in river water samples. The groundwater samples located around the GMWL were the groundwater endmember, with an average $\delta^{18}O$ value of -8.6‰ both for May and October. Substituting the $\delta^{18}O$ values of the two endmembers into the above equation, the results show that the river water proportion in groundwater ranged from 26.5% to 66.2% in May, and from 39.1% to 100% in October (Table 6).

Among these sites, the Longdong (JN20), Baiyunguan (JN18), and Kuangcun (JN51) sites could not receive the recharge from Yufu River based on the topographic and hydrogeological conditions. The enrichment of stable isotopes of these sites may be caused by other recharge sources or different flow paths. Dongkema (JN36) had a river water mixing ratio of 100% in October, which indicates that the streambed of Yufu River in Dongkema section had a strong infiltration capacity. In addition, from the river water proportion, the recharge effect was more obvious in October than in May, which could be proven by: (1) the groundwater samples from four sites, Dongkema (JN4/JN39), Zhongqi (JN6/JN31), Luoer (JN7/8/JN32), and Manzi (JN10/JN30), had higher river water proportions in October than that in May; (2) the Shigu (JN3/37) site did not show mixing with river water in May, while it was recharged by river water in October.

Table 6. The proportion of river water in groundwater samples in May and October.

May				October			
Code	Site	$\delta^{18}\text{O}$ (‰)	ω (%)	Code	Site	$\delta^{18}\text{O}$ (‰)	ω (%)
JN4	Dongkema	−6.89	66.2	JN36	Dongkema	−6.01	100
JN10	Manzi	−7.38	47.2	JN30	Manzi	−7.21	53.8
JN7/JN8	Luoer	−7.62	37.8	JN32	Luoer	−7.35	48.4
JN6	Zhongqi	−7.91	26.5	JN31	Zhongqi	−7.59	39.1
JN20	Longdong	−7.23	53.0	-	-	-	-
JN18	Baiyunguan	−7.62	38.0	-	-	-	-
-	-	-	-	JN43	CuiMa	−6.83	68.3
-	-	-	-	JN45	Xikema	−7.23	53.2
-	-	-	-	JN46	Yinjialin	−7.31	50.1
JN3	Shigu	−8.13	0	JN37	Shigu	−7.48	43.6
-	-	-	-	JN51	Kuangcu	−7.57	39.9

Chloride is typically considered to be conservative, and was used to calculate the mixing proportion of river water in groundwater [6]. However, the similar concentrations in river water (38.4 mg/L) and groundwater (averagely 49.6 mg/L in May and 36.2 mg/L in October) precluded its effectiveness as a tracer to quantify the mixing between river water and groundwater in the Jinan karst system. The efficiency of tracers in quantifying the interaction between river water and groundwater is dependent on the differences in endmember values [4]. The exception was the stable isotope ^{222}Rn , which showed obvious differences in river water and groundwater. However, it was not effective in determining the mixing fractions of river water and groundwater in this study, because ^{222}Rn does not necessarily move conservatively with water.

6. Conclusions

The effects of recharge from streambed of Yufu River on Jinan karst system are evaluated using hydrogeochemistry and stable isotope. The infiltration recharge from streambed changes the chemical and isotopic characteristics of karst groundwater with enrichment of $\delta^{18}\text{O}$ value, decrease of HCO_3^- concentration and NO_3^- concentration, increase of SO_4^{2-} concentration. Jinan karst system could be divided into four zone based on the hierarchical cluster analysis. The effect area of river water recharge is mainly around the streambed of Yufu River. The proportion of river water in groundwater samples around the streambed is calculated by binary mixing model based on $\delta^{18}\text{O}$. The flow path of river water recharge is delineated from the isoline of $\delta^{18}\text{O}$. Along the flow path, the quantitative variations of mineral phases are obtained from inverse chemical modeling.

Author Contributions: Y.G., D.Q., J.S. and L.L. did the preliminary studies, designed and performed the experiments, conducted field studies, analyzed the data, and wrote the paper. F.L. and J.H. help the field investigations.

Funding: This research was funded by National Natural Sciences Foundation of China, grant No. 41172215.

Acknowledgments: This study was funded by the National Natural Sciences Foundation (41172215), the project of pilot technology support scheme on aquatic ecological civilization of Water Resources Department of Shandong Province and Shandong Province Financial Bureau.

Conflicts of Interest: The authors declare no conflict of interest.

References

- Bailly-Comte, V.; Jourde, H.; Pistre, S. Conceptualization and classification of groundwater–surface water hydrodynamic interactions in karst watersheds: Case of the karst watershed of the Coulazou River (Southern France). *J. Hydrol.* **2009**, *376*, 456–462. [[CrossRef](#)]
- Wang, Y.; Ma, T.; Luo, Z. Geostatistical and geochemical analysis of surface water leakage into groundwater on a regional scale: A case study in the Liulin karst system, northwestern China. *J. Hydrol.* **2001**, *246*, 223–234. [[CrossRef](#)]

3. White, W.B. Karst hydrology recent developments and open questions. *Eng. Geol.* **2002**, *65*, 85–105. [[CrossRef](#)]
4. Hamilton, J.; Ford, D. Karst geomorphology and hydrogeology of the Bear Rock Formation—A remarkable dolostone and gypsum megabreccia in the continuous permafrost zone of Northwest Territories, Canada. *Carbonate Evaporite* **2002**, *17*, 114–115. [[CrossRef](#)]
5. Mudarra, M.; Andreo, B. Relative importance of the saturated and the unsaturated zones in the hydrogeological functioning of karst aquifers: The case of Alta Cadena (Southern Spain). *J. Hydrol.* **2011**, *397*, 263–280. [[CrossRef](#)]
6. Hartmann, A.; Goldscheider, N.; Wagener, T.; Lange, J.; Weiler, M. Karst water resources in a changing world: Review of hydrological modeling approaches. *Rev. Geophys.* **2014**, *52*, 218–242. [[CrossRef](#)]
7. Ghasemizadeh, R.; Hellweger, F.; Butscher, C.; Padilla, I.; Vesper, D.; Field, M.; Alshawabkeh, A. Review: Groundwater flow and transport modeling of karst aquifers, with particular reference to the North Coast Limestone aquifer system of Puerto Rico. *Hydrogeol. J.* **2012**, *20*, 1441–1461. [[CrossRef](#)] [[PubMed](#)]
8. Qiao, X.J.; Li, G.M.; Li, Y.P.; Liu, K. Influences of heterogeneity on three-dimensional groundwater flow simulation and wellhead protection area delineation in karst groundwater system, Taiyuan City, Northern China. *Environ. Earth Sci.* **2015**, *73*, 6705–6717. [[CrossRef](#)]
9. Katz, B.G.; Catches, J.S.; Bullen, T.D.; Michel, R.L. Changes in the isotopic and chemical composition of ground water resulting from a recharge pulse from a sinking stream. *J. Hydrol.* **1998**, *211*, 178–207. [[CrossRef](#)]
10. Barbieri, M.; Boschetti, T.; Petitta, M.; Tallini, M. Stable isotope (H-2, O-18 and Sr-87/Sr-86) and hydrochemistry monitoring for groundwater hydrodynamics analysis in a karst aquifer (Gran Sasso, Central Italy). *Appl. Geochem.* **2005**, *20*, 2063–2081. [[CrossRef](#)]
11. Shahul Hameed, A.; Resmi, T.R.; Suraj, S.; Warriar, C.U.; Sudheesh, M.; Deshpande, R.D. Isotopic characterization and mass balance reveals groundwater recharge pattern in Chaliyar river basin, Kerala, India. *J. Hydrol. Reg. Stud.* **2015**, *4*, 48–58. [[CrossRef](#)]
12. Wong, C.I.; Mahler, B.J.; Musgrove, M.; Banner, J.L. Changes in sources and storage in a karst aquifer during a transition from drought to wet conditions. *J. Hydrol.* **2012**, *468*, 159–172. [[CrossRef](#)]
13. Katz, B.G.; Coplen, T.B.; Bullen, T.D.; Davis, J.H. Use of chemical and isotopic tracers to characterize the interactions between ground water and surface water in mantled karst. *Ground Water* **1997**, *35*, 1014–1028. [[CrossRef](#)]
14. Malard, F.; Chapuis, R. Temperature Logging to Describe the Movement of Sewage-Polluted Surface-Water Infiltrating into a Fractured Rock Aquifer. *J. Hydrol.* **1995**, *173*, 191–217. [[CrossRef](#)]
15. Qin, D.J.; Zhao, Z.F.; Guo, Y.; Liu, W.C.; Haji, M.; Wang, X.H.; Xin, B.D.; Li, Y.; Yang, Y. Using hydrochemical, stable isotope, and river water recharge data to identify groundwater flow paths in a deeply buried karst system. *Hydrol. Processes* **2017**, *31*, 4297–4314. [[CrossRef](#)]
16. Cardenal, J.; Benavente, J.; Cruzsanjulian, J.J. Chemical Evolution of Groundwater in Triassic Gypsum-Bearing Carbonate Aquifers (Las-Alpujarras, Southern Spain). *J. Hydrol.* **1994**, *161*, 3–30. [[CrossRef](#)]
17. Zheng, X.Q.; Zang, H.F.; Zhang, Y.B.; Chen, J.F.; Zhang, F.; Shen, Y. A Study of Hydrogeochemical Processes on Karst Groundwater Using a Mass Balance Model in the Liulin Spring Area, North China. *Water-Sui* **2018**, *10*, 903. [[CrossRef](#)]
18. Jones, I.C.; Banner, J.L.; Humphrey, J.D. Estimating recharge in a tropical karst aquifer. *Water Resour. Res.* **2000**, *36*, 1289–1299. [[CrossRef](#)]
19. Aquilina, L.; Ladouche, B.; Dorfliger, N. Recharge processes in karstic systems investigated through the correlation of chemical and isotopic composition of rain and spring-waters. *Appl. Geochem.* **2005**, *20*, 2189–2206. [[CrossRef](#)]
20. Hunt, R.J.; Coplen, T.B.; Haas, N.L.; Saad, D.A.; Borchardt, M.A. Investigating surface water–well interaction using stable isotope ratios of water. *J. Hydrol.* **2005**, *302*, 154–172. [[CrossRef](#)]
21. Su, X.S.; Xu, W.; Yang, F.T.; Zhu, P.C. Using new mass balance methods to estimate gross surface water and groundwater exchange with naturally occurring tracer Rn-222 in data poor regions: A case study in northwest China. *Hydrol. Process.* **2015**, *29*, 979–990. [[CrossRef](#)]
22. Stellato, L.; Terrasi, F.; Marzaioli, F.; Belli, M.; Sansone, U.; Celico, F. Is ²²²Rn a suitable tracer of stream–groundwater interactions? A case study in central Italy. *Appl. Geochem.* **2013**, *32*, 108–117. [[CrossRef](#)]
23. Singh, P.; Chaturvedi, R.K.; Mishra, A.; Kumari, L.; Singh, R.; Pal, D.B.; Giri, D.D.; Singh, N.L.; Tiwary, D.; Mishra, P.K. Assessment of ground and surface water quality along the river Varuna, Varanasi, India. *Environ. Monit. Assess.* **2015**, *187*, 170. [[CrossRef](#)] [[PubMed](#)]

24. Melloul, A.; Collin, M. The Principal Components Statistical-Method as a Complementary Approach to Geochemical Methods in Water-Quality Factor Identification—Application to the Coastal-Plain Aquifer of Israel. *J. Hydrol.* **1992**, *140*, 49–73. [[CrossRef](#)]
25. Cloutier, V.; Lefebvre, R.; Therrien, R.; Savard, M.M. Multivariate statistical analysis of geochemical data as indicative of the hydrogeochemical evolution of groundwater in a sedimentary rock aquifer system. *J. Hydrol.* **2008**, *353*, 294–313. [[CrossRef](#)]
26. Kang, F.X.; Jin, M.G.; Qin, P.R. Sustainable yield of a karst aquifer system: A case study of Jinan springs in northern China. *Hydrogeol. J.* **2011**, *19*, 851–863. [[CrossRef](#)]
27. Chi, G.; Xing, L.; Zhu, H. The study of quantitative relationship between the spring water and the dynamic change of the atmospheric precipitation in Jinan. *Ground Water* **2017**, *39*, 8–11.
28. Wu, X.; Niu, J.; Niu, J. Experimental research on artificial compensation in Yufu River for groundwater to protect springs. *Water Resour. Power* **2003**, *21*, 53–55.
29. Li, B.; Qin, D.; Guo, Y.; Liu, W.; Haji, M.; Lin, L.; Guan, Q. Effect of Yufu River on chemical processes of karst groundwater in Jinan, Shandong Province. *J. Eng. Geol.* **2017**, *25*, 190–198.
30. Plummer, L.N.; Busby, J.F.; Lee, R.W.; Hanshaw, B.B. Geochemical Modeling of the Madison Aquifer in Parts of Montana, Wyoming, and South-Dakota. *Water Resour. Res.* **1990**, *26*, 1981–2014. [[CrossRef](#)]
31. Craig, H. Isotopic Variations in Meteoric Waters. *Science* **1961**, *133*, 1702–1703. [[CrossRef](#)] [[PubMed](#)]
32. Birk, S.; Liedl, R.; Sauter, M. Identification of localised recharge and conduit flow by combined analysis of hydraulic and physico-chemical spring responses (Urenbrunnen, SW-Germany). *J. Hydrol.* **2004**, *286*, 179–193. [[CrossRef](#)]



© 2019 by the authors. Licensee MDPI, Basel, Switzerland. This article is an open access article distributed under the terms and conditions of the Creative Commons Attribution (CC BY) license (<http://creativecommons.org/licenses/by/4.0/>).